Applied Thermal Engineering 181 (2020) 115880

Contents lists available at ScienceDirect

Applied Thermal Engineering

journal homepage: www.elsevier.com/locate/apthermeng

Characteristics of evaporation of propane (R290) in compact smooth and microfinned tubes

Ehsan Allymehr*, Ángel Álvarez Pardiñas, Trygve Magne Eikevik, Armin Hafner

Department of Energy and Process Engineering, NTNU Norwegian University of Science and Technology, Kolbjørn Hejes vei 1D, 7491 Trondheim, Norway

HIGHLIGHTS

- Evaporation of propane studied experimentally in smooth and microfinned tubes.
- Heat transfer coefficient and pressure drop are obtained experimentally.
- Mass flux does not increase heat transfer coefficient in microfinned tubes.
- Predictive methods have different accuracies for different microfinned tubes.

ARTICLE INFO

Keywords:
Hydrocarbon
Refrigeration
Heat transfer
Pressure drop
Microfinned

ABSTRACT

Evaporation of flowing propane and the effect of enhanced geometry on heat transfer coefficient and pressure drop is experimentally investigated. One smooth tube and two microfinned tubes with an outer diameter of 5 mm were tested. Heat transfer coefficient and pressure drop were determined for saturation temperatures of 0, 5 and 10 °C for smooth tube, and the effect of using tubes with enhanced geometries was evaluated at heat fluxes ranging between 15 and 33 kW m^{-2} and mass fluxes between 250 and 500 kW m^{-2} s^{-1}. The increase of heat transfer coefficient for microfinned tubes relative to smooth tube diminishes with increasing mass flux, while the increase of pressure drop remains unaffected. Comparison of the experimental results with correlations for prediction of pressure drop and heat transfer coefficient demonstrates availability of reliable correlations. Nevertheless, correlations show considerable divergence in accuracy for different microfinned tubes.

1. Introduction

The majority of working fluids currently used in refrigeration systems have particularly high global warming potential (GWP) [3]. New refrigeration systems should aim towards fluids of lower GWP while being more efficient in power consumption to reduce both the direct and indirect impact on the environment. Hydrocarbons and, in particular, propane (R290) have long been considered an alternative refrigerant as they have a favorable saturation curve for various applications, low GWP and zero Ozone Depletion Potential (ODP). While Hydrocarbons were used in the first generation of refrigeration systems their application was later limited as a consequence of flammability concerns, specially as the Lower Flammability Limit (LFL) for propane is very low [13]. Although the working fluid charge for a refrigeration system utilizing propane as working fluid can be theoretically half of a comparable system using R134a (the latent heat of vaporization for propane is almost double), this is not enough to satisfy safety regulations in specific applications where higher capacities are required.

Therefore the primary research goal with hydrocarbons has been to reduce the system charge [32]. It has been shown that the majority of the charge in refrigeration systems accumulates in heat exchangers where liquid phase is available with higher density [31]. Consequently, it is essential to decrease the volume of heat exchangers. The use of microfinned tubes provides an opportunity to use hydrocarbon systems with reduced sizes, lower charges and higher capacities by increasing the heat transfer coefficient (HTC) in heat exchangers.

Prior research on evaporation of hydrocarbons has mainly focused on tubes of around 10 mm [37,19,42]. Thonon [40] reviewed the literature on hydrocarbon heat transfer in compact heat exchangers noting that there is a need for more experimental data on in-tube flow boiling of hydrocarbons, especially in the case of microfinned tubes. To the best of our knowledge, the only available reference is Nan & Infante Ferreira [28], where evaporation and condensation of propane in a

* Corresponding author.
E-mail address: ehsan.allymehr@ntnu.no (E. Allymehr).

https://doi.org/10.1016/j.applthermaleng.2020.115880
Received 26 February 2020; Received in revised form 3 August 2020; Accepted 10 August 2020
Available online 01 September 2020

Nomenclature

Greek

δ_{30}	Percentage of predicted values with less than 30% error

Roman

$\dot{m}$	Mass flow [kg s^{-1}]
d_i	Fin tip diameter [m]
i_{lg}	Enthalpy of vaporization [kJ kg^{-1}]
E	Enhancement Factor [–]
G	Mass flux [kg m^{-2} s^{-1}]
HTC	Heat Transfer Coefficient [kW m^{-2} K^{-1}]
I	Efficiency index [–]
ID	Internal Diameter [mm]
MARD	Mean Absolute Relative Deviation [–]
MRD	Mean Relative Deviation [–]
P	Penalization Factor [–]
Q	Heat input [W]
q	Heat flux [kW m^{-2}]
S	Heat exchange area [m^2]
T	Temperature [°C]
x	Vapor quality [–]

Subscripts

in	Inlet conditions
MF	Microfinned
out	Outlet conditions
pre	Preheater section
sat	Saturated condition
test	Test section
W	Wall

smooth, microfinned, and crosshatched tube with OD of 9.52 mm were studied. Their results showed that while the HTC is higher for microfinned tubes compared to smooth tubes, the cross hatched tubes do not make a significant difference; the increase in HTC seems to be more noticeable at higher mass fluxes. Furthermore, correlations for internally enhanced tubes considerably over predicted their experimental data. Pamitran et al. [33] examined the HTC of propane in stainless steel tubes of 1.5 and 3.0 mm inner diameter and developed a correlation based on the experimental results. Maqbool et al. [25] investigated the evaporation of propane in a 1.70 mm ID vertical circular minichannel; they reported most notably that the HTC increases with heat flux and saturation temperature while the effect of mass flux and vapor quality is insignificant. de Oliveira et al. [30] determined HTC and studied flow patterns of propane flowing in a 1.0 mm ID tube at saturation temperature of 25 °C, and the results show a high dependency of HTC on mass flux and heat flux. More recently, Lillo et al. [22] studied the vaporization of R290 in a tube with ID of 6 mm at high saturation temperatures. They noted that the main heat transfer mechanism seems to be nucleate boiling, while correlations of Bertsch et al. [2] and Friedel [11] predicted their results for HTC and pressure drop most accurately. Longo et al. [24] compared the evaporation of R290 and R1270 with R404A in a small diameter tube showing that R404A and R1270 exhibit the highest heat transfer coefficient and lowest pressure drop, while R290 is affected by a particularly low dryout quality. There have also been several studies investigating mixtures of hydrocarbons. Wen & Ho [43] conducted experiments with propane, butane and a mixture of them flowing in a 2.46 mm ID tube, and results showed that the HTC was significantly improved compared to R134a as a working fluid. Zou et al. [46] studied mixtures of R170 and R290 and their evaporation characteristics, proposing a correlation for prediction of HTC. Kedzierski & Kim [17] analyzed heat transfer of various refrigerants and their mixtures, including R290 and R134a, in a 9.64 mm ID tube containing a twisted tape insert.

Several studies have dealt with the effect of enhanced geometries in flow boiling of different fluids. Cho & Kim [6] compared the evaporation characteristics of CO_2 in smooth and microfinned tubes with OD of 9.52 and 5 mm showing that the HTC in microfinned tubes increased by up to 210%, whilst the pressure drop increase was up to 1.9 times. Celen et al. [5] investigated evaporation of R134a in smooth and microfinned tubes, showing that the pressure drop is increased by up to 3

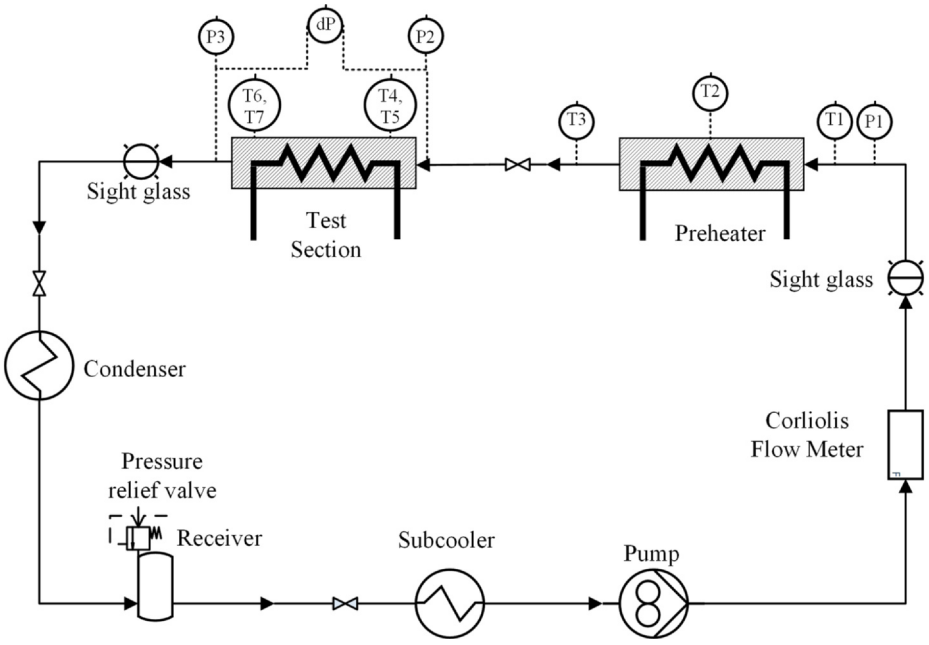

Fig. 1. Test rig schematic.

times while the heat transfer coefficient is increased by 1.9 times. Colombo et al. [9] observed the flow patterns, characteristics of evaporation and condensation of R134a in one smooth and two microfinned tubes showing that both microfinned tubes increase the HTC compared to the smooth tube and found no differences among them. Bandarra Filho et al. [1] compared experimental results for the pressure drop of R134a in smooth and grooved tubes and developed a correlation based on the results.

Thus, while the state of the art for experimental results on evaporation of refrigerants is rather extensive, there seems to be a lack of data regarding different surface enhancements and comparison with smooth tubes specially for hydrocarbons. This paper aims to increase the available information on flow boiling of R290 in compact smooth and microfinned tubes by providing a database of HTC, pressure drop and comparison with relevant correlations. The two microfinned tubes (MF1 and MF2), and the smooth tube have an outer diameter of 5 mm. They were tested at mass fluxes ranging from 250 to 500 kW m^{-2} s^{-1} and the heat flux ranged from 15 to 33 kW m^{-2}. Furthermore, the smooth tube was tested at three saturation temperatures of 0, 5 and 10 °C.

2. Experimental setup

An experimental test rig, located at Thermal lab of the Department of Energy and Process Engineering of Norwegian University of Science and Technology was designed to determine flow boiling HTC and pressure drop of different refrigerants. A schematic of the test rig is shown in Fig. 1. The liquid refrigerant is pumped through the system using an inverter controlled gear pump (Tuthill DGS.68), with a Coriolis mass flow meter (Rheonik RHM 03) that measures the circulated mass flow. Refrigerant is then heated up to the desired vapor quality in the preheater, using an electrical heating cable that is directly wound around the tube. An adiabatic section is located before the test section to ensure fully developed conditions. The adiabatic section consists of two parts: the first is 1 meter long with ID of 8 mm and later a length of 75 mm of the corresponding test tube. Heat input both at preheater and test section is controlled with a Pulse Wave Modulation (PWM) where the input voltage (National Instruments NI-9225) and current (National Instruments NI-9246 and National Instruments NI-9227 for preheater and test section, respectively) is measured at 50 kHz to obtain the power input. The heated test section length is 500 mm and goes through a 30 mm OD copper tube of the same length. An electrical heating cable is wound around the outer tube and the distance between the outer tube and the test tube is filled with tin to distribute the heat evenly along the test section. Tin was melted in by placing tin bars in between the outer tube and test tube while the whole test section was placed vertically and the outer copper tube was heated using a torch. Presence of voids in tin was checked by controlling the final weight of the test section. At the outlet of the test section, a sight glass enables visualizing the flow; as this glass sight did not have the same diameter as the test tube, it was not used for flow pattern recognition. The two valves located upstream of the test section and downstream of the sight glass allow the replacement of test sections in a short time by limiting the effort required for vacuuming the new test section. Nonetheless, the whole test rig was vacuumed and purged with nitrogen for the start up and before any propane was charged. After the sight glass and valve, the propane flows through a condenser and a subcooler cooled by recirculating chillers to ensure a single phase liquid flow to the pump. The saturation pressure of the system is controlled by the set temperature of the chiller connected to the condenser.

To determine the HTC, the wall temperatures were measured with two pairs of Type T thermocouples brazed to the tube wall. Thermocouples were located 100 mm from the inlet and outlet of the heated test section such that in each location, one thermocouple is in contact with the top and the other with the bottom part of the test tube. The fluid saturation temperature was obtained from the saturation pressure; pressure transducers are connected to pressures taps located at the inlet and outlet of the test Section 547 mm away from each other. Pressure drop was measured in diabatic condition directly from the differential pressure transducer connected to the same ports. A photograph of one of the test sections is shown in Fig. 2.

2.1. Tested tubes

Three tubes with OD of 5 mm and different internal geometries were studied. The geometrical parameters of the tubes are detailed in Table 1, and the physical representations of the parameters are presented in Fig. 3. The two microfinned tubes, MF1 and MF2, have roughly the same dimensions for the fins, while the MF2 tube has a higher number of fins and spiral angle, which results in a higher available area for heat transfer compared to the other tubes. A cross sectional view of the two tested microfinned tubes is shown in Fig. 4.

2.2. Uncertainty analysis and validation

Uncertainty analysis was carried out by the method elaborated in ISO [15] with a confidence level exceeding 95% (coverage factor of 2). Utilized instruments are listed in Table 2 with their respective uncertainty. The total average uncertainty for pressure drop was 4.8%, 3.7% and 3.7% for smooth, MF1 and MF2 tube, respectively. For HTC, these values were 3.6%, 6.2% and 9.0% for smooth, MF1 and MF2 tube, respectively. The increase of uncertainty for HTC values in microfinned tubes is caused by the smaller temperature differences between the saturation temperature and wall temperature. Finally, the uncertainty values for average vapor quality is 3.6%, 2.4% and 2.6% for smooth, MF1 and MF2 tube, respectively.

Single phase tests were performed to validate the test facility. Pressure drop and HTC were calculated and compared against Darcy Weisbach formula and the correlation by Gnielinski V.[12], showing an average absolute deviation of 3.7% and 2.6% for pressure drop and heat transfer coefficient, respectively.

The test section was insulated using perlite and then contained by hard insulation. To inspect the effectiveness of the insulation, a thermal camera was used to visualize the temperature distribution and detect any hot spots. Furthermore, several tests were performed at vacuum conditions to evaluate heat leakage at different heat fluxes. The results showed a fairly linear relationship between the temperature difference of the heating element and environment and the heat loss to the

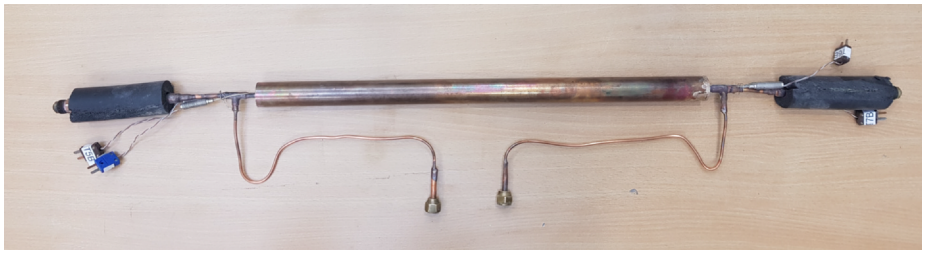

Fig. 2. Photograph of a test section.

Table 1
Geometrical parameters of the test tubes.

	Unit	Smooth tube	MF1	MF2
Outer diameter (OD)	mm	5	5	5
Fin tip diameter (d_i)	mm	4.1	4.32	4.26
Wall thickness (t_w)	mm	0.45	0.22	0.22
Actual cross sectional area	mm^2	13.2	15.7	14.8
Fin height (l_f)	mm	–	0.12	0.15
Fin number (n)	(–)	–	35	56
Fin angle (γ)	°	–	35	15
Spiral angle (β)	°	–	15	37
Heat exchange area ratio	(–)	1	1.51	2.63

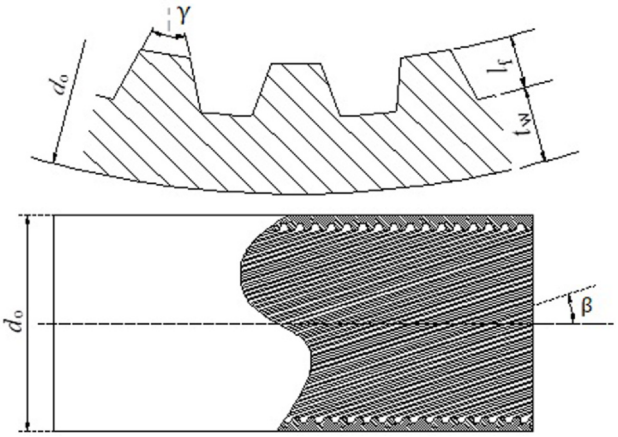

Fig. 3. Physical presentation of the geometrical parameters.

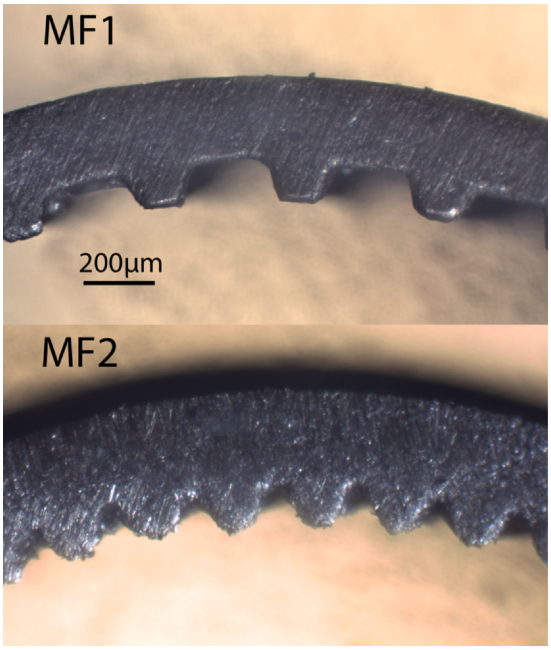

Fig. 4. Cross sectional view of the microfinned tubes.

environment, which was taken into account into calculations by Eq. (1).

$$Q_{loss} = 0.2075 \cdot (T_{element} - T_{amb}) - 0.2925 \quad [W] \tag{1}$$

Heat loss to the environment was on average 3.1% of heat input and the maximum value never exceeded 5.1% in highest heat fluxes.

Table 2
List of instruments and their respective uncertainties.

	Type	Range	Uncertainty
Flow meter	Coriolis	0–5 kg min^{-1}	± 0.1% [a]
Absolute pressure sensor	Strain gauge	0–10 bar	± 0.16% [b]
Differential pressure sensor	Strain gauge	0–0.5 bar	± 0.15% [b]
Thermoucouples	Type T	–	±0.05 K
Preheater	Electrical	3450 W	±0.44% [a]
Test section heater	Electrical	620 W	±0.55% [a]

[a] Of the reading.
[b] Of the set span.

2.3. Data reduction

The system was considered to be in a steady state when the average standard deviation of the four wall temperatures in the last 15 samples was less than 0.1 °C, if this condition was not met, it was considered to be unstable and the data was discarded. The data from the sensors were recorded for over 120 s to obtain 50 samples, which were then averaged. HTC and pressure drop values are reported for an average vapor quality value which is calculated by Eq. (2):

$$x = x_{in} + \frac{\Delta x}{2} = \frac{Q_{pre} - \dot{m} \cdot (i_{sat,l} - i_1)}{\dot{m} \cdot i_{lg(Ppre)}} + \frac{Q_{test} - Q_{loss}}{2 \cdot \dot{m} \cdot i_{lg(Psat)}} \tag{2}$$

wherein i_1 is the enthalpy of subcooled fluid before entering the preheater, P_{pre} is the pressure at the preheater section and P_{sat} is the arithmetic average of the inlet and outlet pressure at the test section.

Heat transfer coefficients were calculated using Eq. (3):

$$h = \frac{Q_{test} - Q_{loss}}{S(\overline{T}_w - \overline{T}_{sat})} \tag{3}$$

where T_{sat} is derived from the saturation pressure, P_{sat}. $\overline{T}_w$ and S are defined as:

$$\overline{T}_w = \frac{1}{4} \sum_{i=1}^{4} T_{w,i} \tag{4}$$

$$S = \pi d_i L \tag{5}$$

For the microfinned tubes, the parameters depending on the ID, such as mass flux and heat flux, were calculated based on a smooth tube with d_i equal to the the fin tip diameter. Thermodynamic properties are evaluated using REFPROP V10 [20].

The total pressure drop ΔP_t is calculated by addition of the momentum pressure ΔP_a drop with frictional pressure drop ΔP_f , given by:

$$\Delta P_a = \Delta P_f + \Delta P_a \tag{6}$$

In order to evaluate the momentum pressure drop, the void fraction was calculated using Rouhani & Axelsson [35] correlation. Although this correlation was originally developed for vertical tubes, it takes into account several parameters that are important in mini and micro channels, therefore it has been used in multiple sources for calculation of the void fraction in horizontal tubes [22,29].

3. Results and discussion

3.1. HTC and pressure drop

Table 3 summarizes the working conditions for the three tubes. In order to analyze the effect of different parameters, tests were performed in varying mass fluxes and heat fluxes for all the tubes while the effect of saturation temperature was evaluated for the smooth tube.

Fig. 5 investigates the effect of saturation temperature on HTC of the smooth tube. Since no relation between the saturation temperature and HTC was discernible, no specific tests were performed in microfinned tubes to study the direct effect of saturation temperature.

Table 3
Operating conditions for experimental setup.

	Unit	Range/Value
Fluid	–	Propane (R290)
Saturation Temperature [T_{sat}]	°C	0, 5, 10
Reduced pressure [P_{red}]	–	0.11–0.15
Heat flux [q]	kW m^{-2}	15, 24, 33
Mass flux [G]	kW m^{-2} s^{-1}	250–500
Tube outer diameter [OD]	mm	5
Vapor quality [x]	–	0.14–1
Quality change [Δx]	–	0.06–0.15

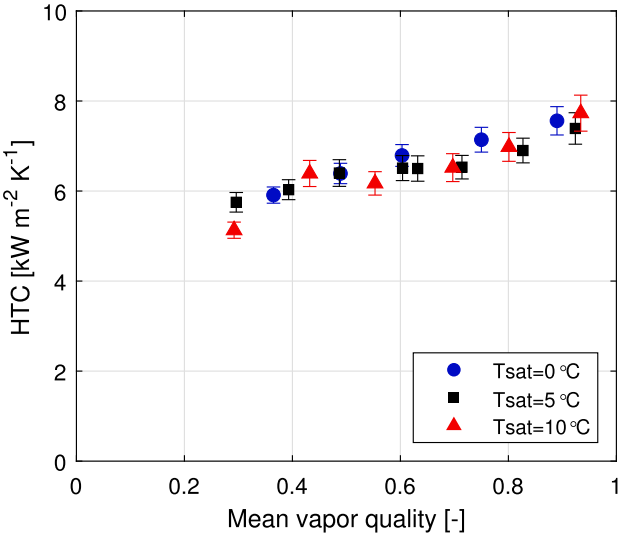

Fig. 5. Effect of saturation temperature on HTC, G = 250 kW m^{-2} s^{-1}, q = 15 kW m^{-2}.

Fig. 6 depicts the effect of heat flux on HTC for the tested tubes. The results show that by increasing the heat flux from 15 kW m^{-2} to 24 kW m^{-2} there is a considerable increase in the HTC in all vapor qualities for all the tested tubes. A further increase of heat flux to 34 kW m^{-2} diminishes the rate of increased HTC in low vapor qualities for all the tubes. In higher vapor quality regions, there is no increase of HTC for the smooth tube and HTC decreases for microfinned tubes compared to a lower heat flux. A closer look at the experimental data showed that the decrease of HTC is mainly caused by the increase in the wall temperature at the inlet section of the test tube. The reason for this remains unclear to the authors, as it would most likely require a flow visualization test to understand the underlying phenomena. Nevertheless, it can be said that this is most probably caused by the geometry of the tube and the complex flow arising from it.

The effect of mass flux on HTC in different tubes can be observed in Fig. 7. HTC increases in the smooth tube with the highest mass flux at high vapor qualities, while the lowest mass fluxes exhibit a rather small increase over the whole vapor quality range, indicating an insignificant contribution from convective heat transfer mechanism. On the contrary, while both of the microfinned tubes show a substantial increase of HTC in higher vapor qualities, the HTC is largely independent of mass flux. It can be argued that the microfinned tubes' fin tips break up the liquid film and readily cause an increase in the turbulence, nullifying the effect of increased turbulence in higher mass fluxes on HTC while higher vapor qualities lead to a thinner liquid film on the wall, thus increasing the HTC.

Unlike HTC, pressure drop exhibits a dependence on saturation temperature (Fig. 8). Pressure drop for T_{sat} = 0 °C is about 30% greater relative to the comparable case of T_{sat} = 10 °C at intermediate vapor qualities. This can be explained by the decrease in the viscosity of the gas phase while the liquid density and liquid viscosity increase, which in turn causes an increase in the superficial velocity of the gas phase and higher shear stress in the liquid phase. The thinning of liquid film at high vapor qualities eliminates the effect of higher shear stress of the liquid phase, and the values for pressure drop seem to converge close to vapor quality of 1.

It can be seen that for all the tested tubes, the most influential factor for pressure drop is the mass flux, presented in Fig. 9. Unsurprisingly, the high HTCs for MF2 tube are coupled with large pressure drops, reaching values of up to 100 kPa m^{-1}. It can also be inferred from Fig. 9 that with the increasing mass flux, the pressure drop increases in the microfinned tubes, while in Fig. 7 it was shown that the increasing mass flux does not result in a higher HTC.

Unlike mass flux, it can be seen in Fig. 10 that the heat flux does not affect the total pressure drop in a meaningful way for any of the tubes.

Colombo et al. [9] defined three parameters to compare the effectiveness of microfinned tubes, Enhancement factor E, Penalization factor P, and efficiency index, I, which are formulated as:

$$E = \frac{h_{MF}}{h_{Smooth}} \tag{7}$$

$$P = \frac{\Delta P_{MF}}{\Delta P_{Smooth}} \tag{8}$$

$$I = \frac{E}{P} \tag{9}$$

These values were calculated at vapor quality of x = 0.45 for different mass fluxes and represented in Fig. 11. The Enhancement factor gradually decreases for both MF1 and MF2, while the penalization factor remains mostly the same over the whole range, therefore diminishing efficiency index at higher mass fluxes. The downward trend

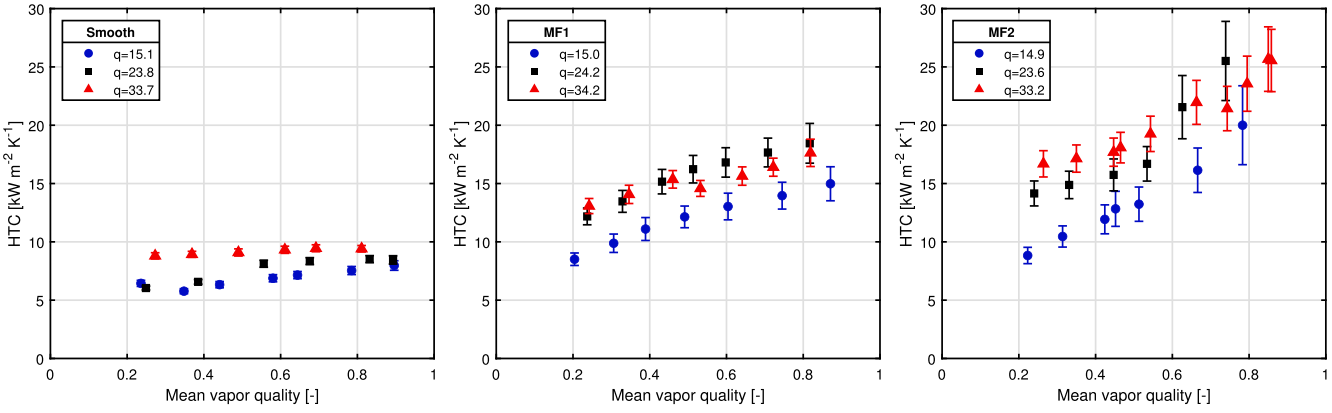

Fig. 6. Effect of heat flux on HTC with G = 300 kW m^{-2} s^{-1}, T_{sat} = 10 °C for three different tubes, heat flux (q) in the legend reported in kW m^{-2}.

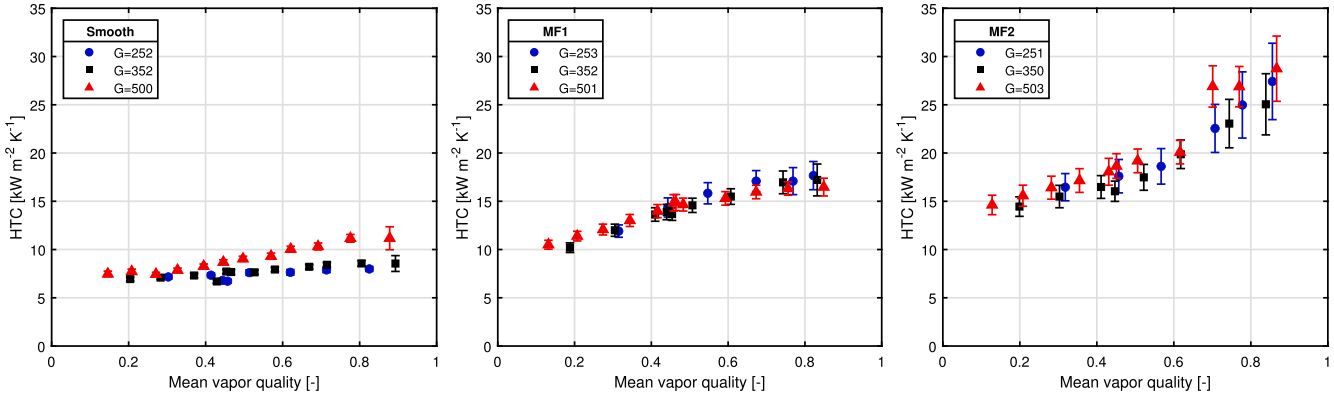

Fig. 7. Effect of mass flux on HTC with q = 23 kW m^{-2}, T_{sat} = 5 °C for three different tubes, mass flux (G) reported in the legend in kW m^{-2} s^{-1}.

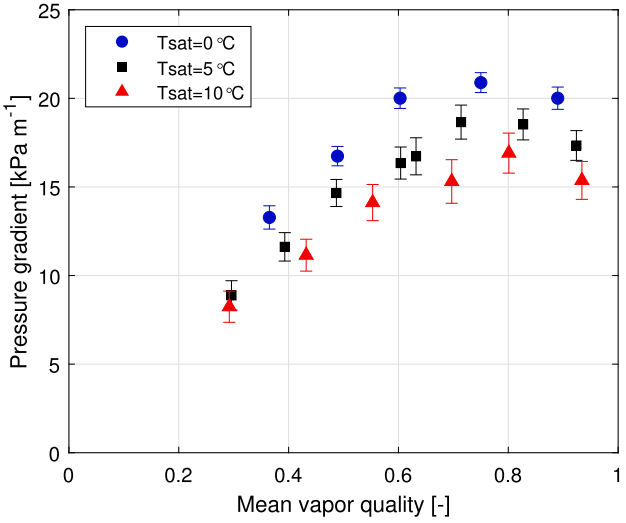

Fig. 8. Effect of saturation temperature on total pressure gradient of smooth tube at q = 23 kW m^{-2}, G = 300 kW m^{-2} s^{-1}.

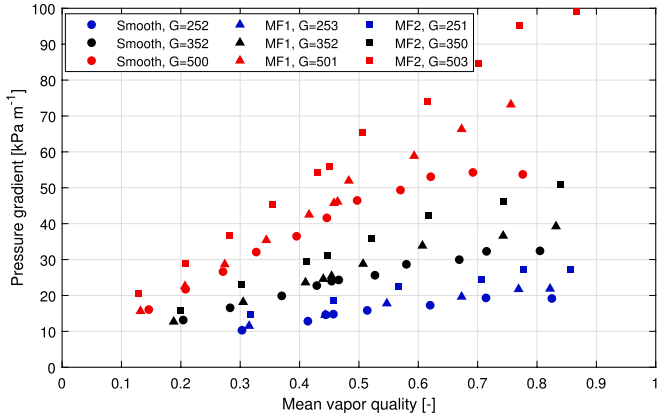

Fig. 9. Effect of mass flux on total pressure gradient at q = 23 kW m^{-2}, T_{sat} = 5 °C for all the tubes, mass flux (G) in kW m^{-2} s^{-1}.

of enhancement factor can be explained by the fact that the rate of increase of HTC for the smooth tube with increasing mass flux is higher than for MF tubes. However, for mass fluxes higher than 400 kW m^{-2} s^{-1}, HTC for smooth tube does not increase anymore. Meanwhile, there is a slight increase for MF tubes; subsequently, the enhancement factor rises. It can be argued that this happens because there is a larger area available for heat exchange in MF tubes. Furthermore, while the enhancement factor and penalization factor for the MF2 tube are higher,

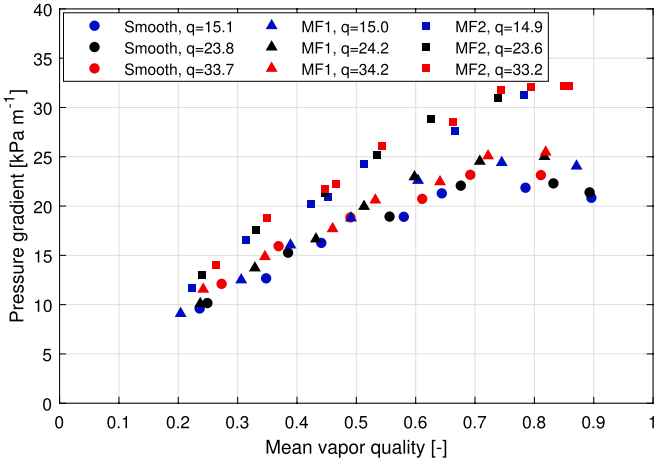

Fig. 10. Effect of heat flux on total pressure gradient at G = 300 kW m^{-2} s^{-1}, T_{sat} = 10 °C for all the tubes, reported heat flux (q) in kW m^{-2}.

the efficiency index for both of the tubes is about the same.

3.2. Correlations

HTC and pressure drop for smooth tubes and microfinned tubes have been comprehensively compared with predictive correlations available in the literature by values of Mean Relative Deviation (MRD) and Mean Absolute Relative Deviation (MARD), defined as:

$$MRD = \frac{100}{n}\sum_{i=1}^{n}\frac{Predicted_i - Experimental_i}{Experimental_i} \quad (10)$$

$$MARD = \frac{100}{n}\sum_{i=1}^{n}\left|\frac{Predicted_i - Experimental_i}{Experimental_i}\right| \quad (11)$$

Additionally, δ_{30} was used as a parameter to show what percentage of the predicted values have less than 30% deviation from the experimental data. Table 4 shows the values of MARD, MAD and δ_{30} of the selected correlations for the smooth tube.

All the studied correlations for the evaluation of pressure drop in smooth tube use dimensionless quantities such as Laplace and Weber number to account for the effect of surface tension except Müller-Steinhagen & Heck [27]. Experimental pressure drop data was most accurately predicted by Xu & Fang [45], where the authors studied correlations and experimental data of 15 different fluids in tubes with hydraulic diameters between 0.81 and 19.1 mm and developed a correlation improving the accuracy especially for micro-channels. All correlations tend to slightly underestimate the experimental data in the low pressure drop range, as can be seen in Fig. 12.

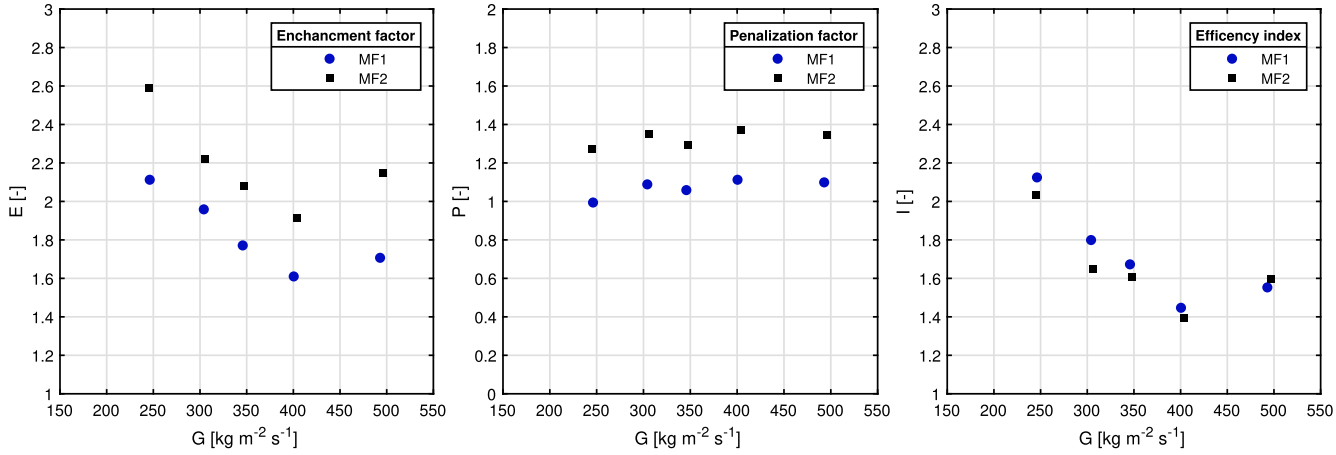

Fig. 11. Enhancement factor *E*, Penalization factor *P* and efficiency index, *I* as a function of mass flux, q = 23 kW m^{-2}, T_{sat} = 5 °C, x = 0.45.

Table 4
Comparison between experimental results and correlation for HTC and pressure drop in smooth tube.

	MRD %	MARD%	δ_{30}
Pressure Drop Correlations			
Müller-Steinhagen & Heck [27]	−21.0	22.4	74.1
Sun & Mishima [38]	−36.9	36.9	12.3
Cavallini et al. [4]	−12.7	20.0	90.1
Xu & Fang [45]	−8.8	11.7	100
Friedel [11]	−22.6	23.0	88.9
HTC Correlations			
Choi et al. [8]	7.2	18.3	88.7
Liu & Winterton [23]	3.5	6.2	100
Kandlikar [16]	12.6	14.4	87.7
Tran et al. [41]	36.3	36.3	25.9
Gungor & Winterton [14]	15.7	16.7	85.2
Shah [36]	−6.2	10.9	100
Li & Wu [21]	−23.9	−26.2	59.3
Kim & Mudawar [18]	−9.2	12.1	97.5
Bertsch et al. [2]	−33.8	33.8	55.6
Lillo et al. [22]	72.5	72.5	48.1
Mohd-Yunos et al. [26]	−41.6	41.6	17.5

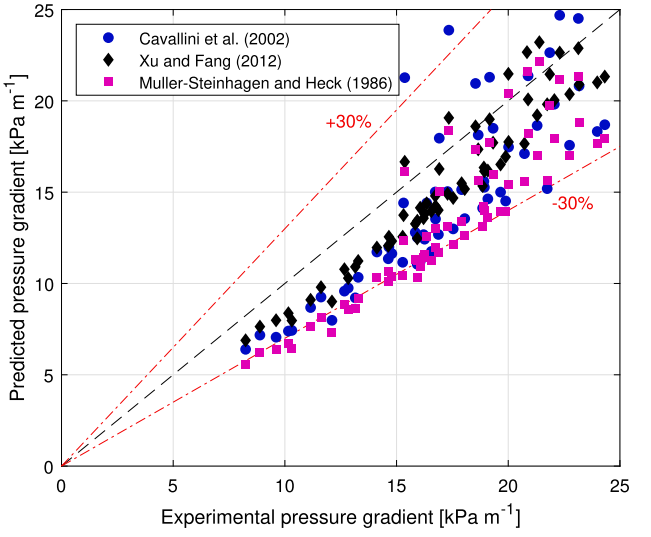

Fig. 12. Comparison between experimental data and correlations of Cavallini et al. [4], Xu & Fang [45], Müller-Steinhagen & Heck [27] for total pressure gradient in smooth tube.

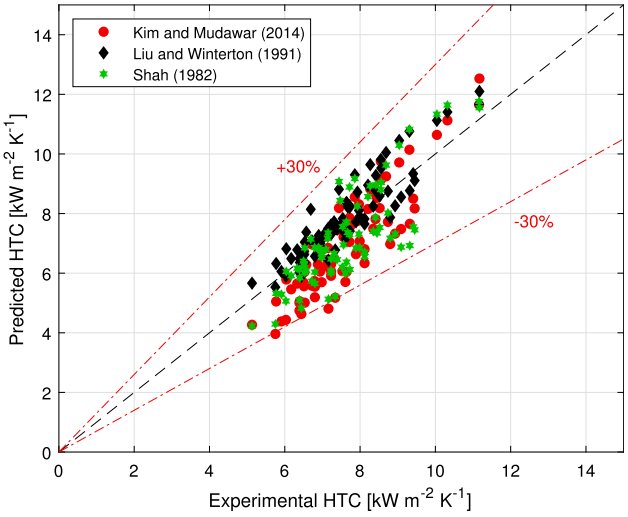

Fig. 13. Comparison between experimental data and correlations of Cavallini et al. [18], Liu & Winterton [23], Shah [36] for prediction of HTC in smooth tube.

Several correlations were studied for the prediction of HTC in smooth tubes. Among them, the recently developed correlation of Mohd-Yunos et al. [26], which has used genetic algorithm to improve the correlations for the prediction of HTC specifically for propane. However, this method seems to fail in accurately predicting the experimental data points in the present study. Lillo et al. [22] has developed another correlation specifically for propane evaporation HTC which is based on Wo jtan et al. [44] correlation. This correlation predicts HTC values in lower vapor qualities reasonably well while the values for higher vapor qualities are greatly over predicted. Correlations of Liu & Winterton [23] and Shah [36] perform best, being able to predict all data points with less than 30% error (Fig. 13).

For the comparison between experimental data for microfinned tubes and correlations it should be noted that for every correlation the HTC or pressure drop was calculated based on the formulation in the respective paper and compared to an equivalent value for experimental data. This is especially important in the choice of diameter and the respective value for the heat transfer area, *S*. The results for MF1 and MF2 are shown in Table 5. The pressure drop correlations of Diani et al. [10] and Rollmann & Spindler [34] exhibit a significant increase in MARD value for MF2 tube compared to MF1. Nevertheless, the correlation by Diani et al. [10] is capable of following the experimental pressure drop data in the whole range for both of the tubes, as depicted on Fig. 14. The gap between the two tubes grows even larger for

Table 5
Comparison between experimental data and correlations for prediction of HTC and pressure drop for microfinned tubes.

	MF1			MF2		
	MAD%	MARD%	δ_{30}	MAD%	MARD%	δ_{30}
Pressure Drop Correlations						
Choi et al. [7]	−26.5	26.5	76.0	22.9	22.9	82.4
Rollmann & Spindler [34]	−6.7	8.7	100	−29.8	29.8	45.1
Diani et al. [10]	1	3	100	−12.7	12.7	100
HTC Correlations						
Tang & Li [39]	−23.8	24.1	72.0	39.0	40.0	33.3
Rollmann & Spindler [34]	−5.2	14.8	100	−26.3	26.3	66.7
Diani et al. [10]	−23.0	23.0	90.0	76.9	76.9	2.0

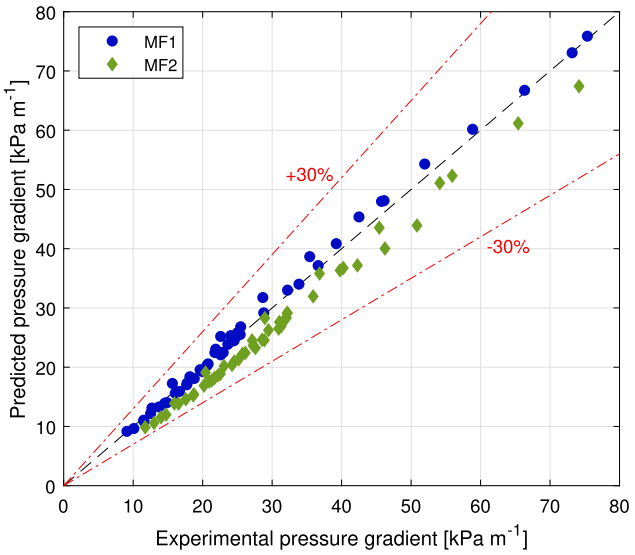

Fig. 14. Experimental total pressure gradient compared to the correlation of Diani et al. [10] for two tested MF tubes.

prediction of HTC for the three correlations considered (Fig. 15), particularly with the correlation of Diani et al. [10]. This can be explained by referring to databases that the prior correlations were built upon which use microfinned tubes that have a much smaller value of heat exchange area ratio compared to MF2 tube.

4. Conclusion

The evaporation of propane in a smooth and two microfinned tubes with 5 mm OD has been studied experimentally. The heat exchange area ratios are 1.51 and 2.63 for MF1 and MF2, respectively. Heat transfer coefficient and pressure drop were determined at saturation temperatures 0, 5 and 10 °C for the smooth tube, while the three tubes were compared at heat fluxes ranging between 15 and 33 kW m^{-2} and mass flux from 250 to 500 kW m^{-2} s^{-1}.

The results were critically compared, noting that saturation temperature does not affect the HTC, but the pressure drop increases with decreasing saturation temperature. With increasing heat flux, HTC increases for all three tubes (indicating a prevalence of nucleate boiling regime), but this increase is restricted to the low vapor quality range for microfinned tubes. The positive effect of mass flux on the HTC for the smooth tube is limited to the highest tested mass flux, demonstrating activation of the convective heat transfer mechanism. The HTC values with microfinned tubes remain the same with increasing mass flux, while the pressure drop increases.

The HTC enhancement comparing microfinned tubes to the smooth tube drops with increasing mass flux, while the relative increase in pressure drop remains more or less the same. Therefore, discouraging the use of MF tube in higher mass fluxes.

Finally, the experimental data has been compared with several predictive correlations available in the literature. For smooth tube correlations of Xu & Fang [45] and Liu & Winterton [23] reliably predict pressure drop and HTC, respectively. For microfinned tube accuracy of the prediction methods varied based on the tested microfinned tube. While pressure drop and HTC for MF1 are reliably predicted by Diani et al. [10] and Rollmann & Spindler [34], respectively, these correlations deviate from experimental data for MF2 tube. This can be explained by the novel design of MF2, where the number of fins and helical angle is rather high.

Declaration of Competing Interest

The authors declare that they have no known competing financial interests or personal relationships that could have appeared to influence the work reported in this paper.

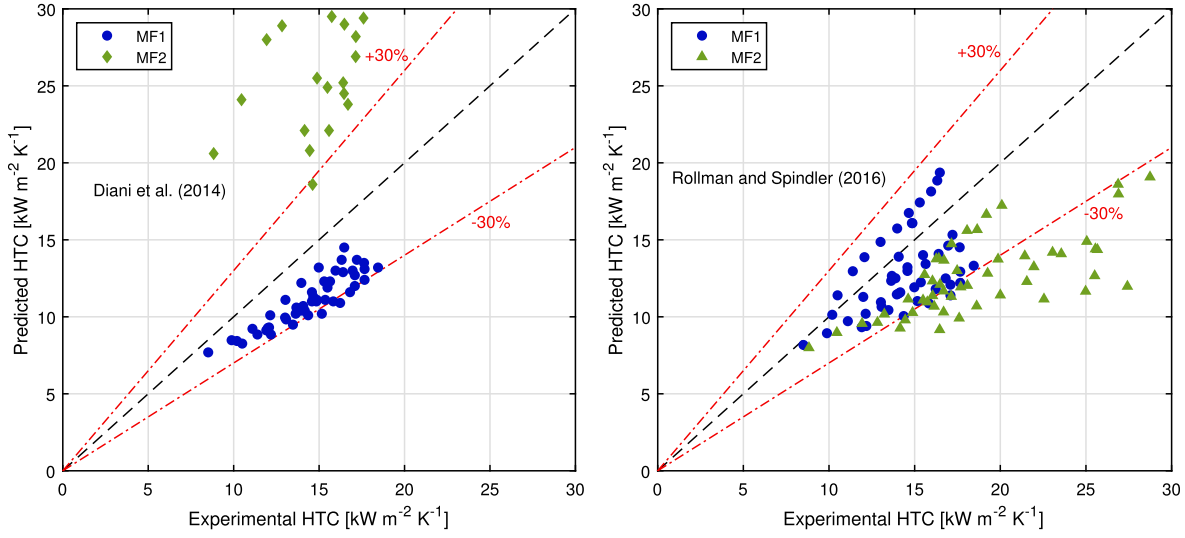

Fig. 15. Prediction of HTC in two microfinned tubes by correlations of Diani et al. [10] and Rollmann & Spindler [34] compared to experimental data.

Acknowledgments

This publication has been funded by HighEFF – Centre for an Energy Efficient and Competitive Industry for the Future, an 8-years' Research Centre under the FME-scheme (Centre for Environment-friendly Energy Research, 257632). The authors gratefully acknowledge the financial support from the Research Council of Norway and user partners of HighEFF.

Appendix A. Calibration process and uncertainty propagation

In order to calibrate the thermocouples, AMETEK JOFRA RTC 157 Reference Temperature Calibrator with the procedure advised by the manufacturer has been used. This unit has an accuracy of 0.04 °C and stability of 0.005 °C. The thermocouples were connected in the same manner as the testing condition (same cables, connections, DAQ) and the values were read each 5 °C in the desired temperature range (-10 °C to 30 °C). The obtained data from the calibration process was used to create a calibration file in LabVIEW.

Below the formulation used for propagating of uncertainty is summarized. Uncertainty for wall temperature:

$$u(T_w) = \sqrt{(1/4)^2 \cdot \sum_{i=4}^{7} u(T_i)} \tag{A.1}$$

Uncertainty for Saturation temperature:

$$u(T_{sat}) = \sqrt{\left(\frac{\partial T_{sat}}{\partial P_{sat}}\right)^2 \cdot u(p_{sat})^2} \tag{A.2}$$

From Antoine equation the relationship between saturation temperature and saturation pressure can be found, by derivation it can be written:

$$\left(\frac{\partial T_{sat}}{\partial P_{sat}}\right) = \frac{803.99}{P_{sat} \cdot (3.9228 - \log_{10}(P_{sat}))} \tag{A.3}$$

Uncertainty for heat transfer coefficient:

$$u(h) = \sqrt{\left(\frac{u(Q_{test})}{T_w - T_{sat}}\right)^2 + \left(\frac{Q_{test} \cdot u(T_w)}{(T_w - T_{sat})^2}\right)^2 + \left(\frac{Q_{test} \cdot u(T_{sat})}{(T_w - T_{sat})^2}\right)^2} \tag{A.4}$$

Uncertainty for inlet vapor quality:

$$u(x_{in}) = \sqrt{\left(\frac{u(Q_{pre})}{\dot{m} \cdot i_{lg(P1)}}\right)^2 + \left(\frac{Q_{pre} \cdot u(\dot{m})}{i_{lg(P1)} \cdot \dot{m}^2}\right)^2} \tag{A.5}$$

Uncertainty for the change in vapor quality:

$$u\left(\Delta x\right) = \sqrt{\left(\frac{u(Q_{test})}{\dot{m} \cdot i_{lg(P_{sat})}}\right)^2 + \left(\frac{Q_{test} \cdot ln(\dot{m}) \cdot u(\dot{m})}{i_{lg(P_{sat})}}\right)^2} \tag{A.6}$$

Uncertainty for the average vapor quality:

$$u(x) = \sqrt{u(x_{in}) + 1/4 \cdot u(\Delta x)^2} \tag{A.7}$$

References

[1] E.P. Bandarra Filho, J.M. Saiz Jabardo, P.E.L. Barbieri, Convective boiling pressure drop of refrigerant R-134a in horizontal smooth and microfin tubes, Int. J. Refrig. 27 (2004) 895–903, https://doi.org/10.1016/j.ijrefrig.2004.04.014.

[2] S.S. Bertsch, E.A. Groll, S.V. Garimella, A composite heat transfer correlation for saturated flow boiling in small channels, Int. J. Heat Mass Transf. 52 (2009) 2110–2118, https://doi.org/10.1016/j.ijheatmasstransfer.2008.10.022.

[3] B. Bolaji, Z. Huan, Ozone depletion and global warming: Case for the use of natural refrigerant – a review, Renew. Sustain. Energy Rev. 18 (2013) 49–54, https://doi.org/10.1016/J.RSER.2012.10.008 https://www.sciencedirect.com/science/article/pii/S1364032112005503.

[4] A. Cavallini, G. Censi, D.D. Col, L. Doretti, G. Longo, L. Rossetto, Condensation of halogenated refrigerants inside smooth tubes, HVAC&R Res. 8 (2002) 429–451, https://doi.org/10.1080/10789669.2002.10391299 http://www.tandfonline.com/doi/abs/10.1080/10789669.2002.10391299.

[5] A. Celen, A. Çebi, A.S. Dalkiliç, Investigation of boiling heat transfer characteristics of R134a flowing in smooth and microfin tubes, Int. Commun. Heat Mass Transf. 93 (2018) 21–33, https://doi.org/10.1016/j.icheatmasstransfer.2018.03.006.

[6] J.M. Cho, M.S. Kim, Experimental studies on the evaporative heat transfer and pressure drop of CO2 in smooth and micro-fin tubes of the diameters of 5 and 9.52 mm, Int. J. Refrig. 30 (2007) 986–994, https://doi.org/10.1016/j.ijrefrig.2007.01.007.

[7] J.Y. Choi, M.A. Kedzierski, P.A. Domanski, Generalized pressure drop correlation for evaporation and condensation in smooth and micro-fin tubes, IIF-IIR-Commission B1 (2001) http://fire.nist.gov/bfrlpubs/build01/PDF/b01078.pdf.

[8] K.-I. Choi, A. Pamitran, C.-Y. Oh, J.-T. Oh, Boiling heat transfer of R-22, R-134a, and CO2 in horizontal smooth minichannels, Int. J. Refrig. 30 (2007) 1336–1346, https://doi.org/10.1016/j.ijrefrig.2007.04.007 https://www.sciencedirect.com/science/article/pii/S014070070700076X?via%3Dihub https://linkinghub.elsevier.com/retrieve/pii/S014070070700076X.

[9] L. Colombo, A. Lucchini, A. Muzzio, Flow patterns, heat transfer and pressure drop for evaporation and condensation of R134A in microfin tubes, Int. J. Refrig. 35 (2012) 2150–2165, https://doi.org/10.1016/j.ijrefrig.2012.08.019 http://www.sciencedirect.com/science/article/pii/S014070071200206X https://www.sciencedirect.com/science/article/pii/S014070071200206X?via%3Dihub https://linkinghub.elsevier.com/retrieve/pii/S01407007120020.

[10] A. Diani, S. Mancin, L. Rossetto, R1234ze(E) flow boiling inside a 3.4 mm ID microfin tube, Int. J. Refrig. 47 (2014) 105–119, https://doi.org/10.1016/j.ijrefrig.2014.07.018.

[11] L. Friedel, Improved friction pressure drop correlation for horizontal and vertical two-phase pipe flow, in: European Two-Phase Flow Group Meeting, Ispra, 1979, pp. 485–492.

[12] V. Gnielinski, New equations for heat and mass transfer in the turbulent flow in pipes and channels, Forsch. Ingenieurwes. 41 (1975) 8–16 http://adsabs.harvard.edu/abs/1975STIA...7522028G.

[13] E. Granryd, Hydrocarbons as refrigerants — an overview, Int. J. Refrig. 24 (2001) 15–24, https://doi.org/10.1016/S0140-7007(00)00065-7 https://www.sciencedirect.com/science/article/pii/S0140700700000657.

[14] K. Gungor, R. Winterton, A general correlation for flow boiling in tubes and annuli, Int. J. Heat Mass Transf. 29 (1986) 351–358, https://doi.org/10.1016/0017-9310(86)90205-X http://linkinghub.elsevier.com/retrieve/pii/001793108690205X.

[15] ISO, Guide to Expression of Uncertainty in Measurement, 1993.

[16] S.G. Kandlikar, A general correlation for saturated two-phase flow boiling heat transfer inside horizontal and vertical tubes, J. Heat Transf. 112 (1990) 219, https://doi.org/10.1115/1.2910348 http://heattransfer.asmedigitalcollection.

asme.org/article.aspx?articleid=1440331.
[17] M. Kedzierski, M. Kim, Convective Boiling and Condensation Heat Transfer with a Twisted-Tape Insert for R12, R22, R152a, R134a, R290, R32/R134a, R32/R152a, R290/R134a, R134a/R600a, 1997. http://fire.nist.gov/bfrlpubs/build97/art030.html.
[18] S.-M. Kim, I. Mudawar, Review of databases and predictive methods for heat transfer in condensing and boiling mini/micro-channel flows, Int. J. Heat Mass Transf. 77 (2014) 627–652, https://doi.org/10.1016/j.ijheatmasstransfer.2014.05.036 https://linkinghub.elsevier.com/retrieve/pii/S0017931014004360.
[19] H. Lee, J. Yoon, J. Kim, P. Bansal, Evaporating heat transfer and pressure drop of hydrocarbon refrigerants in 9.52 and 12.70mm smooth tube, Int. J. Heat Mass Transf. 48 (2005) 2351–2359, https://doi.org/10.1016/j.ijheatmasstransfer.2005.01.012 http://linkinghub.elsevier.com/retrieve/pii/S0017931005001158.
[20] E.W. Lemmon, I.H. Bell, M.L. Huber, M.O. McLinden, NIST Standard Reference Database 23: Reference Fluid Thermodynamic and Transport Properties-REFPROP, Version 10.0, National Institute of Standards and Technology, 2018. doi: https://dx.doi.org/10.18434/T4JS3C. https://www.nist.gov/srd/refprop.
[21] W. Li, Z. Wu, A general criterion for evaporative heat transfer in micro/mini-channels, Int. J. Heat Mass Transf. 53 (2010) 1967–1976, https://doi.org/10.1016/j.ijheatmasstransfer.2009.12.059.
[22] G. Lillo, R. Mastrullo, A.W. Mauro, L. Viscito, Flow boiling heat transfer, dry-out vapor quality and pressure drop of propane (R290): Experiments and assessment of predictive methods, Int. J. Heat Mass Transf. 126 (2018) 1236–1252, https://doi.org/10.1016/j.ijheatmasstransfer.2018.06.069.
[23] Z. Liu, R.H. Winterton, A general correlation for saturated and subcooled flow boiling in tubes and annuli, based on a nucleate pool boiling equation, Int. J. Heat Mass Transf. 34 (1991) 2759–2766, https://doi.org/10.1016/0017-9310(91)90234-6 http://linkinghub.elsevier.com/retrieve/pii/0017931091902346.
[24] G.A. Longo, S. Mancin, G. Righetti, C. Zilio, Hydrocarbon refrigerants HC290 (Propane) and HC1270 (Propylene) low GWP long-term substitutes for HFC404A: a comparative analysis in vaporisation inside a small-diameter horizontal smooth tube, Appl. Therm. Eng. 124 (2017) 707–715, https://doi.org/10.1016/j.applthermaleng.2017.06.080.
[25] M.H. Maqbool, B. Palm, R. Khodabandeh, Investigation of two phase heat transfer and pressure drop of propane in a vertical circular minichannel, Exp. Thermal Fluid Sci. 46 (2013) 120–130, https://doi.org/10.1016/j.expthermflusci.2012.12.002 http://linkinghub.elsevier.com/retrieve/pii/S0894177712003366.
[26] Y. Mohd-Yunos, N. Mohd-Ghazali, M. Mohamad, A.S. Pamitran, J.-T. Oh, Improvement of two-phase heat transfer correlation superposition type for propane by genetic algorithm, Heat Mass Transf. (2019), https://doi.org/10.1007/s00231-019-02776-x http://link.springer.com/10.1007/s00231-019-02776-x.
[27] H. Müller-Steinhagen, K. Heck, A simple friction pressure drop correlation for two-phase flow in pipes, Chem. Eng. Process. 20 (1986) 297–308, https://doi.org/10.1016/0255-2701(86)80008-3 http://users.ugent.be/mvbelleg/literatuurSCHX-StijnDaelman/ORCNext/Supercritical/LiteratureStudy/Literature/PapersSCHeattransfer/Pressuredrop-friction/1986-Muller-Steinhagen-Asimp http://linkinghub.elsevier.com/retrieve/pii/0255270186800083.
[28] X.H. Nan, C. Infante Ferreira, In tube evaporation and condensation of natural refrigrant R290 (Propane), Gustav Lorentz Conf. 290 (2000) 3.
[29] J.D. de Oliveira, J.B. Copetti, J.C. Passos, C.W. van der Geld, On flow boiling of R-1270 in a small horizontal tube: flow patterns and heat transfer, Appl. Therm. Eng. 178 (2020) 115403, https://doi.org/10.1016/j.applthermaleng.2020.115403.
[30] J.D. de Oliveira, J.C. Passos, J.B. Copetti, C.W. van der Geld, Flow boiling heat transfer of propane in 1.0 mm tube, Exp. Thermal Fluid Sci. 96 (2018) 243–256, https://doi.org/10.1016/j.expthermflusci.2018.03.010.
[31] B. Palm, Refrigeration systems with minimum charge of refrigerant, Appl. Therm. Eng. 27 (2007) 1693–1701, https://doi.org/10.1016/j.applthermaleng.2006.07.017 https://linkinghub.elsevier.com/retrieve/pii/S1359431106002481.
[32] B. Palm, Hydrocarbons as refrigerants in small heat pump and refrigeration systems – a review, Int. J. Refrig. 31 (2008) 552–563, https://doi.org/10.1016/j.ijrefrig.2007.11.016 https://linkinghub.elsevier.com/retrieve/pii/S0140700707002216.
[33] A. Pamitran, K.-I. Choi, J.-T. Oh, P. Hrnjak, Characteristics of two-phase flow pattern transitions and pressure drop of five refrigerants in horizontal circular small tubes, Int. J. Refrig. 33 (2010) 578–588, https://doi.org/10.1016/j.ijrefrig.2009.12.009 https://linkinghub.elsevier.com/retrieve/pii/S0140700709002862.
[34] P. Rollmann, K. Spindler, New models for heat transfer and pressure drop during flow boiling of R407C and R410A in a horizontal microfin tube, Int. J. Therm. Sci. 103 (2016) 57–66, https://doi.org/10.1016/j.ijthermalsci.2015.11.010.
[35] S.Z. Rouhani, E. Axelsson, Calculation of void volume fraction in the subcooled and quality boiling regions, Int. J. Heat Mass Transf. 13 (1970) 383–393, https://doi.org/10.1016/0017-9310(70)90114-6 http://linkinghub.elsevier.com/retrieve/pii/0017931070901146.
[36] M.M. Shah, Chart correlation for saturation boiling heat transfer: equation and further study, ASHREA Trans. 88 (1982).
[37] J.Y. Shin, M.S. Kim, S.T. Ro, Experimental study on forced convective boiling heat transfer of pure refrigerants and refrigerant mixtures in a horizontal tube, Int. J. Refrig. 20 (1997) 267–275, https://doi.org/10.1016/S0140-7007(97)00004-2.
[38] L. Sun, K. Mishima, Evaluation analysis of prediction methods for two-phase flow pressure drop in mini-channels, Int. J. Multiph. Flow 35 (2008) 47–54, https://doi.org/10.1016/j.ijmultiphaseflow.2008.08.003 https://catatanstudi.files.wordpress.com/2009/11/2009-evaluation-analysis-of-prediction-methods-for-2-phase-flow-pressure-drop-in-mini-channels_sun.pdf.
[39] W. Tang, W. Li, A new heat transfer model for flow boiling of refrigerants in micro-fin tubes, Int. J. Heat Mass Transf. 126 (2018) 1067–1078, https://doi.org/10.1016/j.ijheatmasstransfer.2018.06.066 https://linkinghub.elsevier.com/retrieve/pii/S0017931018315539.
[40] B. Thonon, A review of hydrocarbon two-phase heat transfer in compact heat exchangers and enhanced geometries, Int. J. Refrig. 31 (2008) 633–642 https://www.sciencedirect.com/science/article/pii/S014070070800039X https://ac.els-cdn.com/S014070070800039X/1-s2.0-S014070070800039X-main.pdf?_tid=7736d389-b443-4b35-8ffb-50ac91ad354f&acdnat=1536823364_5438da16af606309302c7cfda3040a78.
[41] T.N. Tran, M.W. Wambsganss, D.M. France, Small circular- and rectangular-channel boiling with two refrigerants, Int. J. Multiph. Flow 22 (1996) 485–498, https://doi.org/10.1016/0301-9322(96)00002-X.
[42] S. Wang, M. Gong, G. Chen, Z. Sun, J. Wu, Two-phase heat transfer and pressure drop of propane during saturated flow boiling inside a horizontal tube, Int. J. Refrig. 41 (2014) 200–209, https://doi.org/10.1016/j.ijrefrig.2013.03.019 https://linkinghub.elsevier.com/retrieve/pii/S0140700713000741.
[43] M.-Y. Wen, C.-Y. Ho, Evaporation heat transfer and pressure drop characteristics of R-290 (propane), R-600 (butane), and a mixture of R-290/R-600 in the three-lines serpentine small-tube bank, Appl. Therm. Eng. 25 (2005) 2921–2936, https://doi.org/10.1016/j.applthermaleng.2005.02.013 www.elsevier.com/locate/apthermeng https://linkinghub.elsevier.com/retrieve/pii/S1359431105000827.
[44] L. Wojtan, T. Ursenbacher, J.R. Thome, Investigation of flow boiling in horizontal tubes: Part II—Development of a new heat transfer model for stratified-wavy, dryout and mist flow regimes, Int. J. Heat Mass Transf. 48 (2005) 2970–2985, https://doi.org/10.1016/j.ijheatmasstransfer.2004.12.013 https://linkinghub.elsevier.com/retrieve/pii/S001793100500027X.
[45] Y. Xu, X. Fang, A new correlation of two-phase frictional pressure drop for evaporating flow in pipes, Int. J. Refrig. 5 (2012) 2039–2050, https://doi.org/10.1016/j.ijrefrig.2012.06.011 https://www.sciencedirect.com/science/article/pii/S0140700712001570.
[46] X. Zou, M.Q. Gong, G.F. Chen, Z.H. Sun, Y. Zhang, J.F. Wu, Experimental study on saturated flow boiling heat transfer of R170/R290 mixtures in a horizontal tube, Int. J. Refrig. 33 (2009) 371–380, https://doi.org/10.1016/j.ijrefrig.2009.10.013 http://ac.els-cdn.com/S0140700709002473/1-s2.0-S0140700709002473-main.pdf?_tid=55f8bed8-365a-11e7-8107-00000aab0f27&acdnat=1494514907_bfebf6a8c8cf41265734ee5c99ef50a5.